

# Tracing the Nature of Dark Energy with Galaxy Distribution

P. Solevi<sup>1,2</sup> <sup>\*</sup>, R. Mainini<sup>1,2</sup>, S.A. Bonometto<sup>1,2</sup>, A.V. Macciò<sup>3</sup>, A. Klypin<sup>4</sup> & S. Gottlöber<sup>5</sup>

<sup>1</sup> *Physics Department G. Occhialini, Università degli Studi di Milano–Bicocca, Piazza della Scienza 3, I20126 Milano (Italy)*

<sup>2</sup> *I.N.F.N., Sezione di Milano (Italy)*

<sup>3</sup> *Institute for Theoretical Physics, University of Zürich, Winterthurerstrasse 190, CH–8057 Zürich (Switzerland)*

<sup>4</sup> *Astronomy Department, New Mexico State University, Box 30001, Department 4500, Las Cruces, NM 88003-0001*

<sup>5</sup> *Astrophysikalisches Institut Potsdam, An der Sternwarte 16,14482 Potsdam (Germany)*

3 April 2019

## ABSTRACT

Dynamical Dark Energy (DE) is a viable alternative to the cosmological constant. Yet, constructing tests to discriminate between  $\Lambda$  and dynamical DE models is difficult because the differences are not large. In this paper we explore tests based on the galaxy mass function, the void probability function (VPF), and the number of galaxy clusters. At high  $z$  the number density of clusters shows large differences between DE models, but geometrical factors reduce the differences substantially. We find that detecting a model dependence in the cluster redshift distribution is a hard challenge. We show that the galaxy redshift distribution is potentially a more sensitive characteristics. We do so by populating dark matter halos in  $N$ -body simulations with *galaxies* using well-tested Halo Occupation Distribution (HOD). We also estimate the Void Probability Function and find that, in samples with the same angular surface density of galaxies in different models, the VPF is almost model independent and cannot be used as a test for DE. Once again, geometry and cosmic evolution compensate each other. By comparing VPF's for samples with fixed galaxy mass limits, we find measurable differences.

**Key words:** methods: analytical, numerical – galaxies: clusters – cosmology: theory – dark energy

## 1 INTRODUCTION

High redshift supernovae, anisotropies of the cosmic microwave background (CMB), as well as data on the large-scale galactic distribution (Riess et al. 1988, Perlmutter et al 1988, Tegmark et al. 2001, De Bernardis et al 2000, Hanany et al 2000, Halverson et al 2001, Spergel et al 2003, Percival et al. 2002, Efstathiou et al 2002) indicate that  $\sim 70\%$  of the world contents are due to a smooth component with largely negative pressure. This component is dubbed dark energy (DE). Recently Macciò, Governato & Horellou (2005) presented further arguments in favor of DE based on the local ( $\sim 5$ Mpc) Hubble flow of galaxies. The nature of DE is still open for debate. Candidates range from a positive cosmological constant  $\Lambda$  – yielding a  $\Lambda$ CDM cosmology – to models with a slowly evolving self-interacting scalar field  $\phi$  (dynamical DE; Ratra & Peebles 1988; Wetterich 1988) to

even more exotic physics of extra dimensions (e.g., Dvali & Turner 2003).

$\Lambda$ CDM cosmologies are easy to study and fit most data. Unfortunately, to give a physical motivation to the value of  $\Lambda$ , we need a *fine-tuning* of vacuum energy at the end of the last phase transition. To rival the success of  $\Lambda$ CDM other DE models ought to predict observables hardly distinguishable from it, so that discriminatory tests on DE nature are not easy to devise.

Up to now, most tests based on large scale structure dealt with the evolution of the cluster distribution. Using the Press-Schechter-type approximations (Press & Schechter 1974, PS hereafter; Sheth & Tormen, 1999, 2002 ST; Jenkins 2001) the expected dependence of the cluster mass function on DE nature was extensively studied (see, e.g., Wang & Steinhardt 1998, Haiman et al 2001, Majumdar & Mohr 2003, Mainini, Macciò & Bonometto 2003). The results were used to predict the redshift dependence of various observables, such as temperatures ( $T$ ) or photon counts ( $N$ ). In Sec. 2, we compare the (virial) mass functions for different

\* E-mail: solevi@mib.infn.it

DE. An important – and often overlooked – factor is the dependence of halo concentration  $c$  on the DE equation of state. For given virial mass the concentration varies with DE nature up to 80 %, as shown by simulations (Klypin, Macciò, Mainini & Bonometto 2003; Linder & Jenkins 2003; Kuhlen et al. 2005). The model dependence of  $c$  is so strong that it can be used as a possible discriminatory test for strong lensing measurements (Dolag et al 2004, Meneghetti et al 2004, Macciò 2004).

The mass function on galactic  $\sim 10^{12}h^{-1}M_{\odot}$  scales is also interesting for testing models of DE. Yet, there is a complication: to make a prediction we need to know how to generate a distribution of galaxies, not just dark matter halos. There are different ways for doing this. We decided to use recent results on the Halo Occupation Distribution (HOD): a probability to find  $N$  galaxies in a halo of mass  $M$ . The HOD properties have been studied in details (Seljak 2000; Benson 2001; Bullock, Wechsler & Somerville 2002; Zheng et al. 2002; Berlind & Weinberg 2002; Berlind et al. 2003; Magliocchetti & Porciani 2003, Yang, van den Bosch & Mo 2003; van den Bosch, Yang & Mo 2003). Numerical simulations including gas dynamics (White, Hernquist & Springel 2001; Yoshikawa et al., 2001; Pearce et al. 2001; Nagamine et al. 2001; Berlind et al. 2003, Yang et al. 2004) or semi-analytical models of galaxy formation (Kauffmann, Nusser & Steinmetz 1997; Governato et al. 1998; Kauffmann et al. 1999a,b; Benson et al. 2000a,b; Sheth & Diaferio 2001; Somerville et al. 2001; Wechsler et al. 2001; Benson et al. 2003a; Berlind et al. 2003) were used, to find a law telling us how halos split in sub-halos hosting individual galaxies.

We run a series of  $N$ -body simulations with different equations of state. In these models the ratio  $w = p_{de}/\rho_{de}$  of the DE pressure to the energy density varies with  $z$  according to field dynamics. The models considered here are the Ratra-Peebles (RP, Ratra & Peebles 1988) and the models with the supergravity (SUGRA, Brax & Martin 1999, 2001; Brax, Martin & Riazuelo, 2000). Appendix A gives a short summary on these models. Each model is specified by an additional parameter – the energy scale  $\Lambda$  of the self-interacting potential of the scalar field. Here we take  $\Lambda = 10^3\text{GeV}$  for both models. In RP (SUGRA),  $w$  shows slow (fast) variations with  $z$ .

The void probability function is an obvious candidate for discriminating models. Fluctuations grow differently in the models. So, one may expect some differences in VPF. We use galaxy distributions to estimate the void probability function (VPF) at different redshifts. While measuring VPF in simulations is straightforward, mimicking observations is slightly more complicated because it requires corrections for geometrical effects and because the answer depends on a definition of galactic populations. At  $z = 0$  no model dependence of the VPF is expected or found. Predictions at higher  $z$  depend on how galaxy samples are defined. In particular, we show that, if equal angular density samples are considered, VPF results are independent of the DE nature. On the contrary, if we select samples above fixed galactic mass  $M$ , a significant signal is found, which can be useful for testing the DE nature.

The plan of the paper is as follows: In Sec. 2 we discuss how geometry and galactic evolution affect the redshift distributions of galaxies and clusters. In Sec. 3 and 4 we discuss the simulations and prescriptions of populating halos with

galaxies. In Sec. 5 and 6 results on redshift distributions and the VPF are given. Sec. 7 is finally devoted to discussing our results and future perspectives.

## 2 GEOMETRICAL AND EVOLUTIONARY FACTORS

Let us consider a set of objects whose mass function is  $n(>M, z)$ . In a spatially flat geometry, their number between  $z$  and  $z + \Delta z$ , in a unit solid angle, is given by

$$N(>M, z, \Delta z) = \int_z^{z+\Delta z} dz' D(z') r^2(z') n(>M, z') \quad (1)$$

with  $D(z) = dr/dz$ . For flat models:

$$D(z) = \frac{c}{H_o} \sqrt{\frac{\Omega_m(z)}{\Omega_{mo}(1+z)^3}}, \quad r(z) = \int_0^z dz' D(z') \quad (2)$$

Here  $\Omega_m(z)$  is the matter density parameter at the redshift  $z$ . The Friedman equation can be written in the form

$$H^2(z) = \frac{8\pi}{3} G \frac{\rho_{mo}(1+z)^3}{\Omega_m(z)} = H_o^2 \frac{\Omega_{mo}(1+z)^3}{\Omega_m(z)}. \quad (3)$$

Along the past light cone,  $a dr = -c dt$ . So, by dividing the two sides by  $dz = -da/a^2$ , one finds that  $a dr/dz = a^2 c dt/da$ . Accordingly,  $D(z) = dr/dz = c/H(z)$  is derived from eq. (3).

When  $w$  is a constant, a useful expression

$$D^2(z) = (c/H_o)(1+z)^{-3} [\Omega_{mo} + (1 - \Omega_{mo})(1+z)^{3w}]^{-1} \quad (4)$$

can be obtained, which allows one to see that the geometrical factors increase both when  $w$  decreases and  $\Omega_{mo}$  decreases in models with  $w < 0$ .

An extension to dynamical DE can be performed either by using the interpolating expressions yielding  $\Omega_m(z)$ , for RP and SUGRA models, provided by Mainini et al (2003b) or, equivalently, through direct numerical integration. We obtain the geometrical factor  $r^2(z)D(z)$  shown in the upper panel of Fig. 1.

Here  $\Omega_{mo} = 0.3$  or  $0.2$  for  $\Lambda\text{CDM}$ , while  $\Omega_{mo} = 0.3$  for SUGRA and RP models (for whom  $\Lambda = 10^3\text{GeV}$ ).  $H_o$  is  $70\text{ km/s/Mpc}$  in all models ( $h = 0.7$ ). In the absence of number density evolution, the upper panel of Fig. 1 shows the dependence of the angular number density on  $z$ .

In the PS formulation, the expected differential cluster number density  $n(M)$ , at a given time, is then given by the expression

$$f(\nu)\nu d \log \nu = \frac{M}{\rho_m} n(M) M d \log M. \quad (5)$$

Here  $\rho_m$  is the matter density,  $\nu = \delta_c/\sigma_M$  is the *bias factor*,  $M$  is the mass scale considered.  $\sigma_M$  is the r.m.s. density fluctuation on the scale  $M$  and  $\delta_c$  is the amplitude that, in the linear theory, fluctuations have in order that, assuming spherical evolution, full recollapse is attained exactly at the time considered (in a standard CDM model this value is  $\sim 1.68$ ; the difference, in other model, ranges around a few percent). As usual, we took a Gaussian  $f(\nu)$  distribution.

Together with eq. (5), we must take into account the virialization condition, which yields significantly different density contrasts  $\Delta_v$  in different DE models. Further details can be found in Mainini et al (2003a).

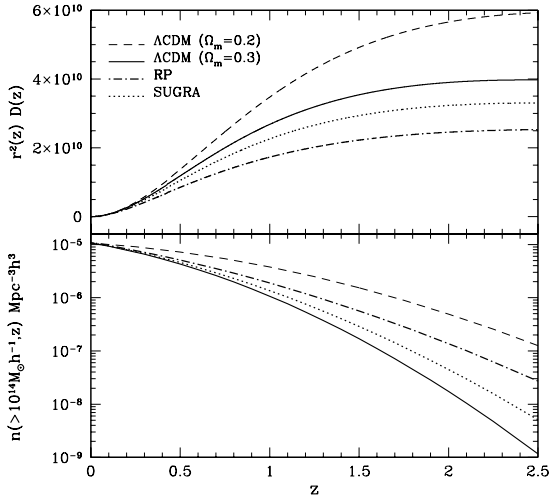


**Figure 1.** Geometrical and evolutionary terms on the cluster mass scale. In both panels  $\Lambda$ CDM with  $\Omega_{m0} = 0.2$  is above  $\Lambda$ CDM with  $\Omega_{m0} = 0.3$ . On the contrary, in the upper and lower panels RP and SUGRA lay on the opposite sides of  $\Lambda$ CDM. In the latter case, cancellation between geometrical and evolutionary effects is therefore expected.

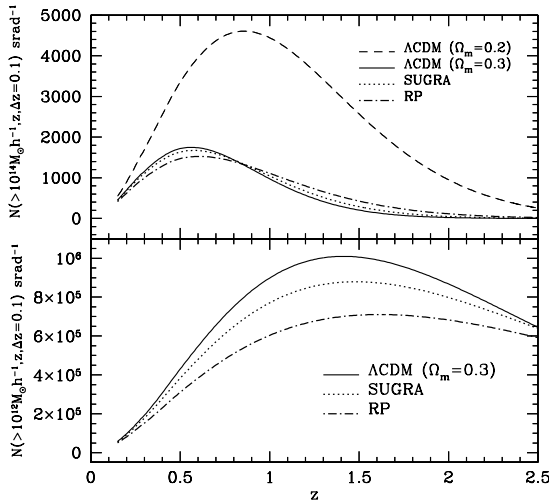


**Figure 2.** The upper panel shows how the redshift distribution on the cluster mass scale depends on the models. The cancellation expected from Fig. 1 has occurred and the models with  $\Omega_{m0} = 0.3$  are quite close, while  $\Lambda$ CDM grants large differences when varying  $\Omega_{m0}$ . In the lower panel, similar curves are shown for halos on galactic mass scales. In this case, evolution is almost model independent and the geometrical factor causes an appreciable difference. On these scales a lower  $\Omega_{m0}$  yields a different halo density, unless the spectrum is normalized to unphysical levels. Hence, only models with  $\Omega_{m0} = 0.3$  are shown.

In the lower panel of Fig. 1 we show the evolution of the number of halos of mass  $> 10^{14} h^{-1} M_{\odot}$ , in comoving volumes. All models are normalized to the same cluster number today and the redshift dependence of  $n(> M, z)$  is clearly understandable, on qualitative bases: When  $\Lambda$ CDM models are considered, the evolution is faster as we approach standard CDM. On the contrary, RP and SUGRA yield a slower evolution than  $\Lambda$ CDM.

The important issue is that, while both the geometrical factor and the evolutionary factor of  $\Lambda$ CDM (with  $\Omega_{m0} = 0.2$ ) lay above  $\Lambda$ CDM (with  $\Omega_{m0} = 0.3$ ), RP and SUGRA factors lay on the opposite sides of  $\Lambda$ CDM.

When the two factors are put together this causes the effect shown in the upper panel of Fig. 2, a strong signal on  $\Omega_{m0}$  and a widespread cancellation for DE models, compared to  $\Lambda$ CDM. Discriminating between different DE natures, from this starting point, is unavoidably a hard challenge.

Geometrical factors do not depend on the mass scale. Instead, evolutionary factors are known to have a stronger dependence on the model for larger masses. As cancellation is almost complete on cluster scales, it is to be expected that geometrical factors yield a significant signal on lower mass scales. This is shown on the lower panel of Fig. 2, where halos of  $10^{12} h^{-1} M_{\odot}$  are considered. A halos of this mass is expected to host a normal galaxy. More massive halos are expected to host many galaxies. Hence, this plot cannot be directly compared with observations. Its main significance is that such lower mass scales deserve to be inspected because DE signals are expected to be strong enough on these scales.

### 3 SIMULATIONS

The simulations run for this work are based on a  $\Lambda$ CDM model and two dynamical DE models, with the same matter density and Hubble parameters ( $\Omega_{m0} = 0.3$  and  $h = 0.7$ ). The simulations are run using the Adaptive Refinement Tree code (ART; Kravtsov, Klypin & Khokhlov 1997). The ART code starts with a uniform grid, which covers the whole computational box. This grid defines the lowest (zeroth) level of resolution of the simulation. The standard Particles-Mesh algorithms are used to compute density and gravitational potential on the zeroth-level mesh. The ART code reaches high force resolution by refining all high density regions using an automated refinement algorithm. The refinements are recursive: the refined regions can also be refined, each subsequent refinement having half of the previous level's cell size. This creates a hierarchy of refinement meshes of different resolution, size, and geometry covering regions of interest. Because each individual cubic cell can be refined, the shape of the refinement mesh can be arbitrary and match effectively the geometry of the region of interest.

The criterion for refinement is the local density of particles: if the number of particles in a mesh cell (as estimated by the Cloud-In-Cell method) exceeds the level  $n_{\text{thresh}}$ , the cell is split (“refined”) into 8 cells of the next refinement level. The refinement threshold may depend on the refinement level. The code uses the expansion parameter  $a$  as the time variable. During the integration, spatial refinement is accompanied by temporal refinement. Namely, each level of refinement,  $l$ , is integrated with its own time step

$\Delta a_l = \Delta a_0/2^l$ , where  $\Delta a_0$  is the global time step of the zeroth refinement level. This variable time stepping is very important for accuracy of the results. As the force resolution increases, more steps are needed to integrate the trajectories accurately. Extensive tests of the code and comparisons with other numerical  $N$ -body codes can be found in Kravtsov (1999) and Knebe et al. (2000).

The code was modified to handle DE of different types, according to the prescription of Mainini et al. (2003b). Modifications include effects due to the change in the rate of the expansion of the Universe and on initial conditions, keeping into account also spatial fluctuations of the scalar field before they enter the horizon.

In this paper we use 4 new simulations. The models are normalized assuming  $\sigma_8 = 0.9$ . They are run in a box of  $100 h^{-1} \text{Mpc}$ . We use  $256^3$  particles with mass  $m_p = 4.971 \cdot 10^9 h^{-1} M_\odot$ . The nominal force resolution is  $3 h^{-1} \text{kpc}$ . All models are spatially flat, while  $\Omega_{m_0} = 0.3$  and  $h = 0.7$ . The two  $\Lambda\text{CDM}$  models start from different random numbers and are indicated as  $\Lambda\text{CDM1}$  and  $\Lambda\text{CDM2}$ . The two DE models, named RP3 and SUGRA3, are started from the same random numbers of  $\Lambda\text{CDM1}$ .

#### 4 GALAXIES IN HALOS

Halos were found in simulations by the same spherical overdensity (SO) algorithm used in Klypin et al (2003). The algorithm locates all non-overlapping largest spheres where the density contrast attains a given value  $\Delta_v$ . Density contrasts are assigned the virialization values, which depend on the redshift  $z$  and on parameters of the DE. For instance, at  $z = 0$ ,  $\Delta_v = 101.0$  for  $\Lambda\text{CDM}$ , 119.4 for SUGRA3 and 140.1 for RP3;  $\Delta_v$  values for higher  $z$  can be found in Mainini, Macciò & Bonometto (2003; see also Mainini et al 2003b).

Figure 3 shows the halo mass function in the  $\Lambda\text{CDM1}$ , the SUGRA3, and the RP3 models at  $z = 0$ . Differences between the models are only due to different  $w(z)$ , while their  $\sigma_8$  is identical. Accordingly, at  $z = 0$  their mass functions almost overlap and are well fitted by the Sheth-Tormen (ST, Sheth & Tormen, 1999) approximation.

However, when we consider galaxies, we need to use another approach because individual halos may host many galaxies of different mass and luminosity. In order to assign galaxies to halos we use a HOD. This is a relatively novel approach to locate galaxies in each halo. It can be used in different ways. Full-scale semi-analytical methods can predict such quantities as the luminosity, colors, star-formation rates. Unfortunately, many important mechanisms are still poorly understood making the results less reliable. It seems therefore advisable to minimize the physical input, keeping just to gravitational dynamics.

In this paper we use a prescription consistent with the results of Kravtsov et al (2004). We utilize an analytical expression recently proposed by Vale & Ostriker (2004), but parameters of the approximation are different from Vale & Ostriker (2004) and tuned to produce a good fit to results of Kravtsov et al (2004). The approximation is based on the assumption that the probability  $P_s(N_s|M)$  for a halo of mass  $M$  to host  $N_s$  subhalos is approximately universal. We take the Schechter approximation

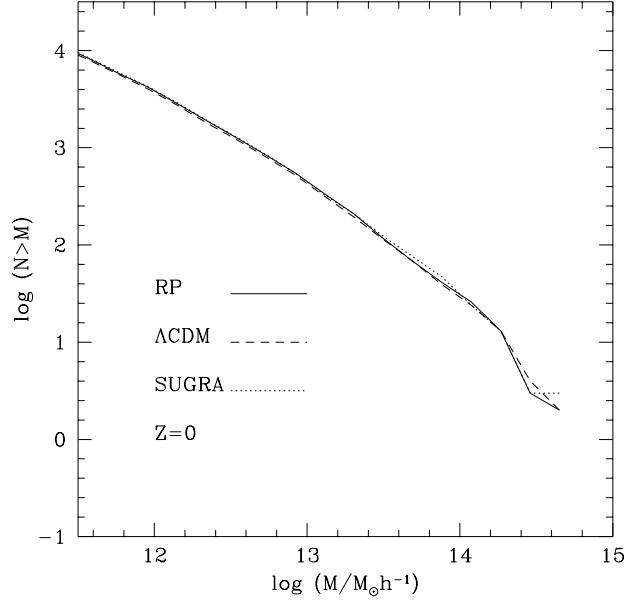


**Figure 3.** Halo mass function at  $z = 0$ . Results for  $\Lambda\text{CDM}$  (dashed line), RP (solid line), and SUGRA (dotted line) overlap.

$$N(m|M) dm = A \frac{dm}{\beta M} \left( \frac{m}{\beta M} \right)^{-\alpha} \exp\left(-\frac{m}{\beta M}\right) \quad (6)$$

for the number of subhaloes with masses in the range  $m$  to  $m + dm$ , for a parent halo of mass  $M$ .  $A$  must be such that the total mass in subhaloes,  $\int_0^\infty dm m N(m|M)$ , is a fraction  $\gamma M$  of the parent halo mass. Therefore  $A = \gamma/\beta\Gamma(2 - \alpha)$ , so that the number of sub-halos of mass  $m$  is

$$n_{sh}(m) = \int_0^\infty dM N(m|M) n_h(M), \quad (7)$$

( $n_h(M)$  is the halo mass function) independently from the parent halo mass. The expression (6) yields the following number of subhaloes with mass  $> m$  in a halo of mass  $M$ :

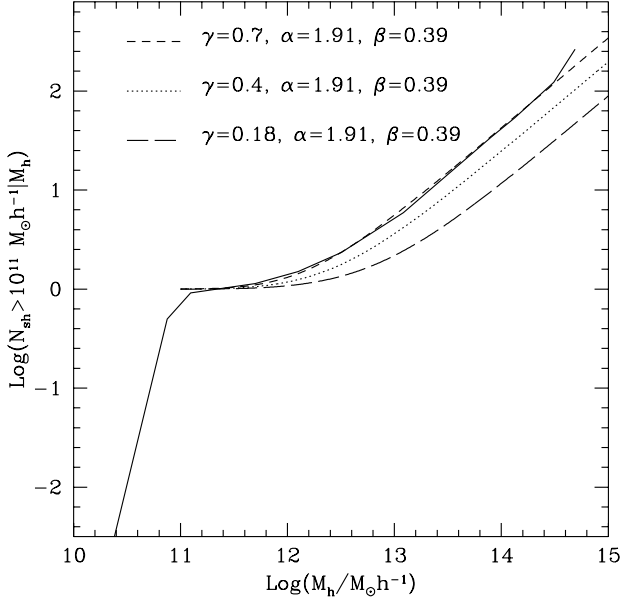
$$N_{sh}(> m, M) = \frac{\gamma}{\beta\Gamma(2 - \alpha)} \int_{m/\beta M}^\infty dx x^{-\alpha} \exp(-x). \quad (8)$$

Figure 4 shows that the expression approximates the results of Kravtsov et al (2004) once we fit parameters  $\alpha, \beta, \gamma$  and add to the expression (8) a unity, *i.e.* the halo as a sub-halo of itself. In a different context, Vale & Ostriker (2004) use the value  $\gamma = 0.18$ ,  $\beta = 0.39$ . Owing to the use we make of eq. (8),  $\gamma = 0.7$  appears more adequate.

If the (differential) halo mass function  $n_h(M)$  is known, the sub-halo mass function is

$$N_{sh}(> m) = \frac{\gamma}{\beta\Gamma(2 - \alpha)} \times \int_{m/\gamma}^\infty dM n_h(M) \int_{m/\beta M}^\infty dx x^{-\alpha} \exp(-x). \quad (9)$$

If we perform nonlinear predictions,  $n_h(M)$  is obtained from the expression (5) or from the corresponding expressions in the ST case. When we deal with simulations, halo masses have discrete values  $m_\nu = \nu m_p$ , appearing  $n_h^{(\nu)}$  times, up to



**Figure 4.** Comparison of different halo occupation distributions. The solid line is the HOD given by Kravtsov et al (2004). Other curves are obtained from eq.(8) for different parameters  $\gamma$  as indicated in the plot.

a top mass  $\nu_M m_p$ . Then

$$N_{sh}(> m) = \frac{\gamma}{\beta \Gamma(2 - \alpha)} \times \sum_{\nu = \frac{m}{\gamma m_p}}^{\nu_M} n_h^{(\nu)} \int_{\nu m / \beta M}^{\infty} dx x^{-\alpha} \exp(-x). \quad (10)$$

In Figure 5 we plot the galaxy mass function obtained with eq. (10) using the mass function of halos in the simulations at  $z = 0$ . We also plot a Schechter function with the parameters shown in the plot best approaching simulation outputs. As expected, the two curves are close. In fact, there must be some relation between masses and luminosities, but the  $M_g/L_g$  ratio should not be a constant.

## 5 GALAXY ANGULAR DENSITY IN MODELS WITH DIFFERENT DE

Let us now consider the galaxy mass function at higher  $z$ , for the different models. According to eq. (1), the number of galaxies with mass  $> m$ , in a solid angle  $\Delta\theta^2$  ( $\Delta\theta \ll 1$ ), between redshifts  $z$  and  $z + \Delta z$ , is

$$\frac{N_g(> m, z; \Delta z, \Delta\theta)}{\Delta z \Delta\theta^2} \simeq c \frac{r^2(z)}{H(z)} n_g(> m, z), \quad (11)$$

if  $n_g(> m, z)$  is the comoving number density of galaxies with mass  $> m$  at a redshift  $z$ . The galaxy density can be obtained from the subhalo mass functions (9) and (10). Accordingly, the average angular distance  $\theta_{gg}$  is given by

$$\theta_{gg}(> m, z) \sqrt{\Delta z} \simeq \frac{1}{r(z)} \left[ \frac{H(z)}{n_g(> m, z)} \right]^{1/2}. \quad (12)$$

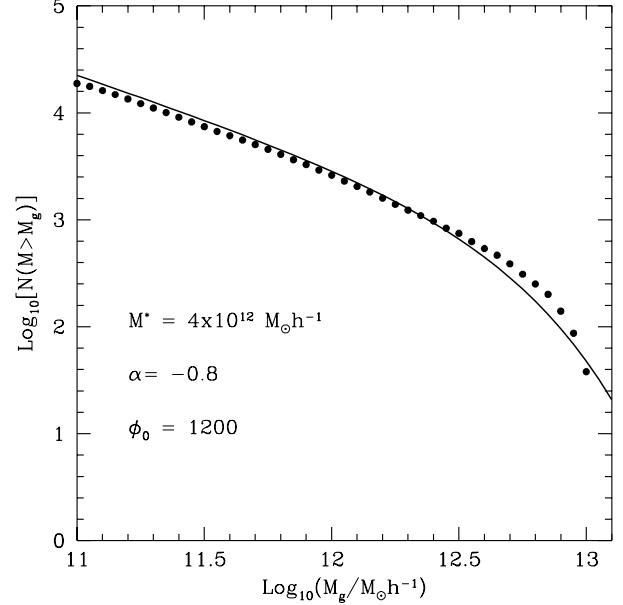


**Figure 5.** Galaxy (cumulative) mass function at  $z = 0$  from simulations (dots) vs. an integral Schechter function, with  $\Phi_0$ ,  $\alpha$  and  $M_*$  shown in the frame.

Thus, the l.h.s. expression is independent of the particular volume considered.

Such  $\theta_{gg}(> m, z)$  therefore depends on geometry, halo mass function and HOD. We however expect that the redshift dependence mostly arises from geometry, while evolution plays a significant role at higher  $z$ . In fact, the main difference between this and the cluster case is that evolution is mild and discrepancies between models, in comoving volumes, up to  $z \sim 2$ , are even weaker.

Let  $\theta_\Lambda(z)$ ,  $\theta_{SU}(z)$ ,  $\theta_{RP}(z)$  be the mean angular distances between galaxies at redshift  $z$  for the  $\Lambda$ CDM, SUGRA and RP models, respectively. Besides these functions, let us also consider the angular distance  $\theta_{geo}(z)$  obtained from eq. (12), keeping the value of  $n_g(> m, z = 0)$  at any redshift and the  $\Lambda$ CDM geometry. Therefore,  $\theta_{geo}(z)$ , although the symbol has no reference to  $\Lambda$ CDM, describes the behavior of the angular separation in a  $\Lambda$ CDM model, in the limit of no halo evolution.

In Figure 6, we compare results obtained from simulations with the ST predictions in different models. Rather than presenting  $\theta_{mod}(z)$ , we plot the fractional difference  $(\theta_{mod} - \theta_{geo})/\theta_{geo}$ . In principle, error bars can be evaluated in two ways: (i) by comparing  $\Lambda$ CDM1 with  $\Lambda$ CDM2 (cosmic variance) and (ii) by comparing the differences between models. The latter can be done only at present because the models have the same power spectrum only at  $z = 0$ . The differences between models exist because the fluctuations grow differently in the past. At larger  $z$ , this *evolutionary variance* should be smaller, but is not easy to evaluate. We use differences between models at  $z = 0$  as a rough estimate of error bars at all redshifts. Judging by the differences between  $\Lambda$ CDM1 and  $\Lambda$ CDM2, the cosmic variance seems to be smaller by a factor of three than the evolutionary differences. We find similar behaviour for different galaxy masses. In all cases, differences between models can be clearly seen.

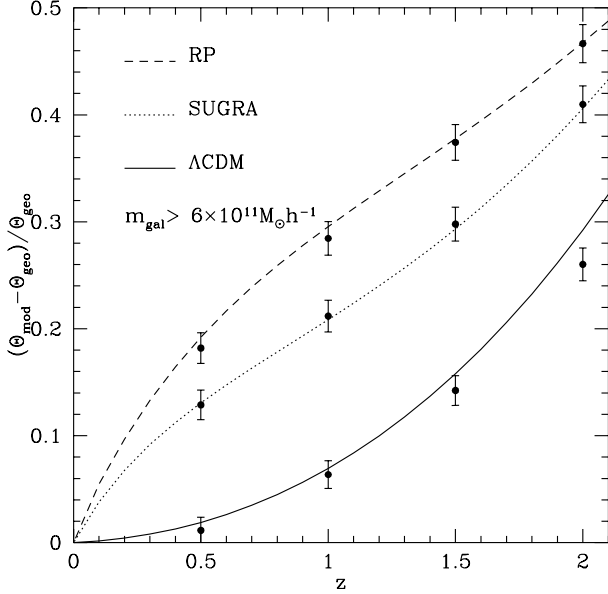


**Figure 6.** The redshift dependence of the mean fractional angular separation in different models. Points with error bars show results of simulations. Curves indicate ST predictions. The plot shows a strong dependence of the galaxy redshift distribution on the DE nature.

The largest differences between models are attained at  $z \sim 1$ . Let us remind that the plot shows the fractional differences between DE models and the  $z$ -dependence due to the mere  $\Lambda$ CDM geometry. At  $z \simeq 1$ , this difference is just  $\simeq 5\%$  for  $\Lambda$ CDM while, for SUGRA, it is  $\sim 20\%$ , because of the different geometry and a still slower cosmological evolution. Even larger is the difference with RP. This compares with an overall variance hardly exceeding  $\sim 2\%$ , if the effective comoving volume inspected is  $\sim 10^6 h^{-3} \text{Mpc}^3$ . For  $\Delta z \sim 0.1$ , this corresponds to  $\delta\theta \sim 30\text{--}40^\circ$ .

The robustness of this discrimination was tested against two observational uncertainties: (i) A possible error of the redshift, up to 5% of the galaxies. (ii) An error of galaxy mass, as we describe below.

The (i) point was tested by dividing the volume  $L^3$  of the box into cells of side  $10^{-1}L$ , with volume  $10^{-3}L^3$ . 50 such cells were selected at random at each redshift and replaced by the cells at the closest redshift considered with their galaxy contents. The redshift displacement between the original cell and its replacements is  $\pm 0.5$ . For a change of 5% in galaxy contents the average shift of  $\theta_{gg}$  is  $\sim 1.2\%$ , laying below the error bars shown in Figure 6.

Let us discuss the (ii) point. We assume that the mean  $M_g/L_g$  ratio is known and that its evolutionary effects are under control. We tested our results against wide fluctuations about average, by individual objects. To do so we allow random *errors* in the cut due to the mass threshold. More in detail, we start from the sample of galaxies obtained through the HOD, at each redshift, and each galaxy mass ( $m$ ) is relaxed by a mass  $m' = m + \Delta m R$ , where  $R$  is a random number with a normal distribution and unity variance. For the sake of example, we took  $\Delta m = 0.8m$ , but replaced all  $m' < 0.1m$  with  $0.1m$ , as well as all  $m' > 1.9m$

with  $1.9m$ , so to preserve the total galaxy mass in the box. We re-estimated  $\theta_{mod}\sqrt{\Delta z}$  using the new masses, for the same mass limits as before. We compare the changes obtained in this way with the Poisson uncertainty, due to the finite number of galaxies in each sample and find that the error obtained from the above procedure ranges between 20 and 40% of the Poisson error. This is perhaps the strongest source of possible errors, but however translates into errors which seldom exceed 3%, if  $\Delta z \sim 0.1z$ , up to  $z = 2$ . Adding together all the possible error sources considered, which are intrinsically independent, we expect overall error bars hardly exceeding 3.8%.

Accordingly, a galaxy sample reasonably including all galaxies with mass  $> 6 \cdot 10^{11} h^{-1} M_\odot$ , up to  $z \sim 1$  and within a solid angle of  $(15^\circ)^2$ , would produce reliable model discrimination.

## 6 THE VOID PROBABILITY FUNCTION

The Void Probability Function (VPF) is defined for objects with mass above a given threshold  $M_{tr}$ . Spheres of various radii  $R$  are then randomly thrown in space and the probability  $P(R)$  of finding them empty is the VPF for  $M_{tr}$ .

When dealing with galaxy samples obtained at  $z = 0$  we expect and find no model dependence of the VPF's. For galaxy distributions at  $z > 0$ , the critical issue is how to define a sample. This can be done either by determining galaxy masses from data, and then by selecting objects with masses above  $M_{tr}$ . Alternatively, one can take the most *luminous* objects down to a fixed angular number density. The latter choice does not require a relation of  $L_g$  with  $M_g$  for individual galaxies. The only condition is that the relation between  $L_g$  and  $M_g$  is monotonic. The effects of a spread around such dependence can then be estimated.

Clearly, each value of  $M_{tr}$ , for each  $z$  and  $\Delta z$ , yields a value of  $\theta_{gg}$  or  $\nu_{gg}$  (mean angular density). These values, as is shown by Fig. 6, are significantly different for different models. *Viceversa*, if we keep, for that  $z$  and  $\Delta z$ , a fixed  $\nu_{gg}$ , the value of  $M_{tr}$  will be different in different models. Results therefore depend on how the threshold is set. Clearly, results are more easily obtainable with the latter threshold definition. Let us also notice that, in the case of no evolution, the  $\Lambda$ CDM curve should coincide with the abscissa. Up to  $z \simeq 0.5$ , the evolution, in fact, is quite modest and only at  $z \simeq 1$  evolution overcomes  $\sim 5\%$ . In principle, VPF's can be directly evaluated in the comoving volumes where galaxies are set. This is however inadequate to compare different models. The fair procedure amounts to the following steps: (i) From cartesian coordinates  $\bar{x}_i$  ( $i = 1, 2, 3$ ) in comoving volumes we pass to the values of  $z$ ,  $\theta$ ,  $\phi$  that an observer, set at  $z = 0$ , would measure. This operation is made by using the right geometry corresponding to the model. Of course, in order to estimate VPF, the real data, giving the  $z$ ,  $\theta$ ,  $\phi$  of each galaxy, must be translated into cartesian coordinates  $x_i$ . An observer, however, does not know the model and can only perform such translation by using the geometry of a *fiducial* model, *e.g.*,  $\Lambda$ CDM.

(ii) The second step therefore amounts to re-transform  $z$ ,  $\theta$ ,  $\phi$  into cartesian coordinates  $x_i$ . These coordinates will coincide with the original ones only for the  $\Lambda$ CDM case. For

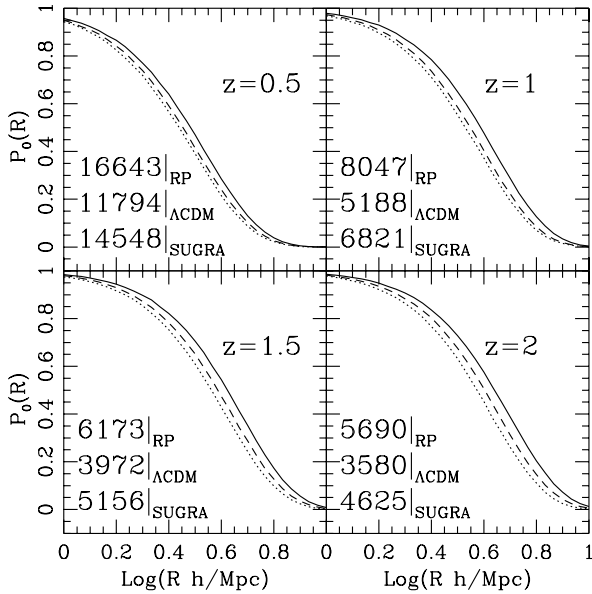


**Figure 7.** VPF's in comoving volumes for fixed angular density. The four panels refer to redshift 0.5, 1, 1.5, 2, as indicated in the frames. The galaxy numbers in the simulation box are reported, for each model and redshift.

other models, they will be significantly different. Let us indicate the space, where galaxies are so set, as *fiducial* space. (iii) We then estimate the VPF using such *distorted* coordinates in the fiducial space and compare the results.

Hence, VPF estimates in comoving volumes can be formally compared, but this comparison bears no observational relevance. The effective comparison shall be performed in the fiducial space.

In spite of that, our outputs can be more easily understood if we first report results in the comoving space. Let us remind that evolutionary differences, up to  $z \sim 2$ , on the galaxy mass scale, are modest. Accordingly, VPF model differences, for galaxies with mass  $> M_{tr}$ , are just marginally discrepant (we omit to plot them). On the contrary, significant differences arise if we do not use equal  $M_{tr}$ 's for all models, but indirect mass limits, corresponding to fixed  $\theta_{gg}$ . In this case, differences do not arise from intrinsic VPF discrepancies, but are induced by  $\theta_{gg}$  discrepancies. In Fig. 7 these differences are shown.

The VPF's obtained in respect of comoving coordinates bear a strict analogy with the mass functions in comoving volumes. The fact that geometry erases almost any signal on the cluster mass function is analogous to what happens for the VPF, when we pass from the comoving to the fiducial space.

In fact, almost all differences between models, found in the comoving space, for galaxy sets corresponding to equal  $\theta_{gg}$ 's, are erased. This is shown in Fig. 8 and Fig. 9 at  $z = 0.5$  and  $z = 2$ . The lack of signal is confirmed by a comparison between the VPF's of various models and the VPF for a Poisson sample with an equal number of points.

The cancellation between geometrical and  $\theta_{gg}$  effects, shown in Fig. 8, indicates that the passage from comoving to fiducial coordinates bears a weight comparable with the

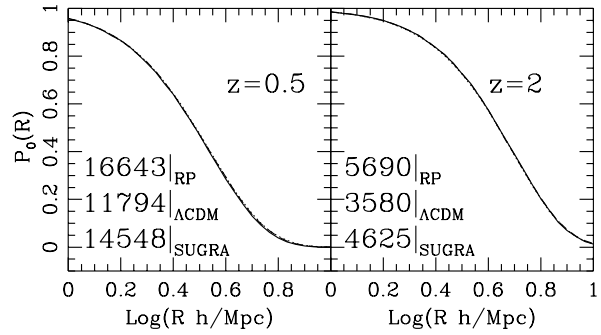


**Figure 8.** VPF's in fiducial volumes for fixed angular density. Upper panels give the VPF's. The tenuous residual differences are magnified in the next plot (Fig. 9), where the differences between model VPF's and the VPF's for a Poisson point sample are plotted. Numbers in the frames as for Fig. 7.

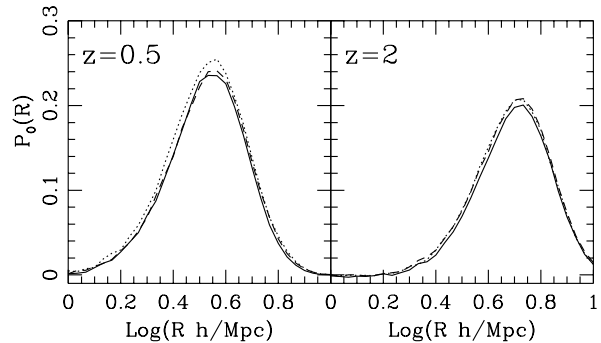


**Figure 9.** Residuals difference between models for VPF in fiducial volumes for fixed angular density (Fig. 8).

differences shown in Fig. 7. It therefore comes as no surprise that VPF's, for samples defined with the same  $M_{tr}$ , almost absent in the comoving space, are significant in the fiducial space. They are shown in Fig. 10.

All the VPF's shown in the previous figures were estimated on the basis of  $\Lambda$ CDM1. Differences between  $\Lambda$ CDM1 and  $\Lambda$ CDM2 are however so small that they could not be appreciated in the above plots. Accordingly, sample variance should not be a relevant limit to the use of VPF's.

The main difficulty in the use of the results shown in Fig. 10 therefore arises from the relation between  $M_g$  and  $L_g$ . If we assume that an average  $M_g/L_g$  ratio is known, as a function of  $L_g$ , we can estimate such difficulties by replacing the sharp threshold on  $M_g$  with a soft threshold, replacing each galaxy mass  $M_g$  with  $M_g + \Delta M_g R$ , as in the previous section. This test was performed for samples as wide as those in our  $100 h^{-1}$  Mpc box and the effects of such replacement are modest, amounting to  $\sim 10\%$  of the difference found between  $\Lambda$ CDM and SUGRA.

This test leaves however open the question of a possible systematic dependence of the average  $M_g/L_g$  ratio on the evolutionary rate and, therefore, on DE nature. This aspect will be deepened in future work.

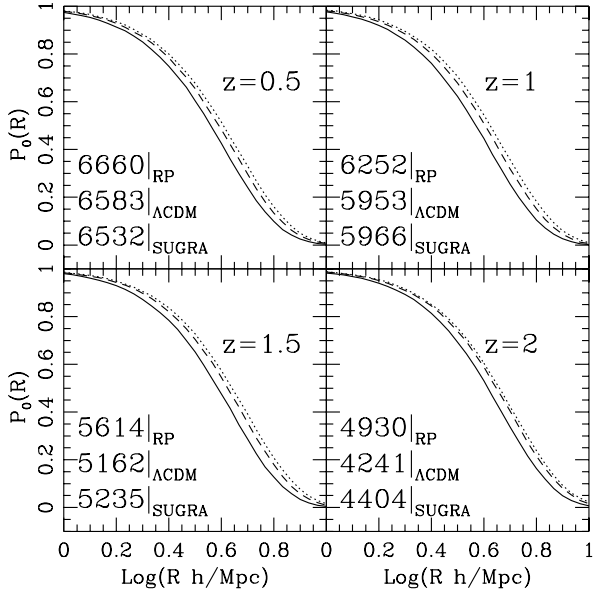


**Figure 10.** VPF’s in fiducial volumes for fixed mass limit (see text). Numbers in the frames as for Fig. 7.

## 7 CONCLUSIONS

Dark Energy modifies the rate of cosmic expansion in the epoch when a substantial fraction of fluctuations on cluster scales reach their turnaround. Therefore, it seems quite natural to trace the redshift dependence of  $w(z) = p_{de}/\rho_{de}$  using the cluster mass function at different redshifts.

Unfortunately, the situation is more complicated. The evolution of  $w(z)$  affects on observations in two ways. First, it causes objects to form and evolve with different rate. Second, it results in different mapping of comoving coordinates of galaxies to observed angular positions and redshifts. Then, on a cluster mass scale ( $\sim 10^{14}h^{-1}M_{\odot}$ ), the evolutionary and geometrical effects tend to cancel, which makes clusters somewhat problematic for testing the equation of state.

In this paper we suggest to use scales where the evolutionary effects are minimized, so that the geometrical effects leave a clearer imprint. In a sense, this is not a new procedure: an analogous idea is utilized when the DE equation of state is tested by using a *standard candle*. Obviously, galaxies are not standard candles themselves, but they can provide a “standard meter” through their (almost) model-independent abundance and evolution.

Previous analysis, which focused on clusters, tried to overcome the above difficulties by making recourse to various features. For example, the evolutionary dependence on  $w$  is preserved if one considers masses *well* above  $10^{14}h^{-1}M_{\odot}$ . Unfortunately, clusters with masses  $\sim 10^{15}h^{-1}M_{\odot}$  or larger are rare today and surely are even more rare in the past. Some analysis (see, *e.g.*, Haiman et al. 2000) stressed a possible role of very massive clusters at large  $z$ . Yet, the number of such clusters cannot be large and, thus, comparing such predictions with observations is a hard challenge. There is also another problem with using cluster masses. Usually the mass function is estimated with a PS-like approximations,

which are well tested with simulations. The “virial” radius  $R_v$  is defined so that inside  $R_v$  the density contrast is  $\Delta_v$ . The value of  $\Delta_v$  depends on the redshift and on DE model. On the contrary, data are typically analyzed with a standard density contrast  $\Delta_c \simeq 180$  (or 200). Increasing  $\Delta_c$  reduces the amplitude of the mass function. If mass functions defined with variable  $\Delta_v$  (almost) overlap one another, mass functions defined with constant  $\Delta_c$  can be different. In order to account for these differences in the definitions, one needs to assume some shape for the density profile in the outskirts of clusters. This is typically done by using a NFW profile with concentration  $c_s \simeq 5$ . As we deal with rather peripheral (virial) cluster regions, we can neglect the spread of actual values of concentration. However, when different  $w(z)$  are considered, the *mean*  $c_s$  changes substantially, up to 80% (Klypin et al 2003; Kuhlen et al. 2005). The differences between  $M_{200}$  and  $M_v$  are not large – 10–15%. Approximately the same percent of the difference depends on  $w$ . This may be still important. Neglecting these corrections may lead to substantial systematic errors.

In order to avoid these and other problems of galaxy clusters, hardly negligible because the cluster signal is intrinsically small, we suggest an alternative approach: to use galactic distribution and to exploit its dependence on the DE nature. In order to use galaxies one needs to know how to treat subhalos of more massive halos because a large fraction of galaxies is hosted by subhalos. To populate massive halos with galaxies we use recent results on the halo occupation distribution (HOD). The DE nature hardly plays a role in halo splitting, but this has never been tested. Dealing with galaxies also requires knowledge of their masses  $M_g$  and (optical) luminosities  $L_g$ . The  $M_g - L_g$  relation is more complex than the relation between  $M_v$ , X-ray flux, and  $T$  in clusters. We emphasize that our analysis does not require a  $M_g - L_g$  relation for individual galaxies, which would depend on other properties of galaxies (*e.g.*, merging history, morphological type, and so on). We need only a *mean* conversion relation; some scatter does not affect the results.

Most of our results are presented in terms of galaxy masses  $M_g$ . One still needs to implement conversion to luminosities before predictions can be compared with observations. This can imply further complications since the  $M_g/L_g$  ratio could depend on  $z$ . In addition, a slight influence of the equation of state of DE on this dependence cannot be excluded.

The differences between DE models for galaxies are much stronger than for clusters and we expect that it will be easier to overcome minor systematic trends. Moreover, our analysis shows that the validity of the assumed mean  $M_g/L_g$  ratio can be tested by looking at the VPF estimated for samples with fixed angular surface number density of galaxies. In fact, predictions of VPF do not depend on DE nature (see Fig. 8). They depend only on the assumed average  $M_g/L_g$  ratio.

In this paper we also discuss various tests based on the void probability function. Besides of finding that the VPF is almost model independent when estimated for a sample with constant angular surface number density of galaxies, we find visible differences for samples with fixed galaxy masses.

Combining the simulated halo distribution with the HOD provides an effective tool for testing the equation of state of DE. More work is needed to define the  $L_g - M_g$  rela-

tion and to reduce systematic effects. It is justified to expect that deep galaxy samples will allow us to constrain the DE nature more reliably than using galaxy clusters.

**Acknowledgments:** We thank Lorin Colombo for stimulating discussions. A.K. acknowledges financial support of NSF and NASA grants to NMSU. S.G. acknowledges financial support by DAAD. Our simulations were done at the LRZ computer center in Munich, Germany.

## APPENDIX A: DYNAMICAL DARK ENERGY MODELS

Dynamical DE is to be ascribed to a scalar field,  $\phi$ , self-interacting through an effective potential  $V(\phi)$ , whose dynamics is set by the Lagrangian density:

$$\mathcal{L}_{DE} = -\frac{1}{2}\sqrt{-g}(\partial^\mu\phi\partial_\mu\phi + V(\phi)) . \quad (\text{A1})$$

Here  $g$  is the determinant of the metric tensor  $g_{\mu\nu} = a^2(\tau)dx_\mu dx_\nu$  ( $\tau$  is the conformal time). In this work we need to consider just a spatially homogeneous  $\phi$  ( $\partial_i\phi \ll \dot{\phi}$ ;  $i = 1, 2, 3$ ; dots denote differentiation with respect to  $\tau$ ); the equation of motion is then:

$$\ddot{\phi} + 2\frac{\dot{a}}{a}\dot{\phi} + a^2\frac{dV}{d\phi} = 0 . \quad (\text{A2})$$

Energy density and pressure, obtained from the energy-momentum tensor  $T_{\mu\nu}$ , are:

$$\rho = -T_0^0 = \frac{\dot{\phi}^2}{2a} + V(\phi) , \quad p = \frac{1}{3}T_i^i = \frac{\dot{\phi}^2}{2a} - V(\phi) , \quad (\text{A3})$$

so that the state parameter

$$w \equiv \frac{p}{\rho} = \frac{\dot{\phi}^2/2a - V(\phi)}{\dot{\phi}^2/2a + V(\phi)} \quad (\text{A4})$$

changes with time and is negative as soon as the potential term  $V(\phi)$  takes large enough values.

The evolution of dynamical DE depends on details of the effective potential  $V(\phi)$ . Here we use the model proposed by Ratra & Peebles (1988), that yield a rather slow evolution of  $w$ , and the model based on supergravity (Brax & Martin 1999, 2001; Brax, Martin & Riazuelo 2000). The latter gives a much faster evolving  $w$ . The RP and SUGRA potentials

$$V(\phi) = \frac{\Lambda^{4+\alpha}}{\phi^\alpha} \quad RP, \quad (\text{A5})$$

$$V(\phi) = \frac{\Lambda^{4+\alpha}}{\phi^\alpha} \exp(4\pi G\phi^2) \quad SUGRA \quad (\text{A6})$$

cover a large spectrum of evolving  $w$ . These potentials allow tracker solutions, yielding the same low- $z$  behavior that is almost independent of initial conditions. In eqs. (A5) and (A6),  $\Lambda$  is an energy scale in the range  $10^2$ – $10^{10}$  GeV, relevant for the physics of fundamental interactions. The potentials depend also on the exponent  $\alpha$ . Fixing  $\Lambda$  and  $\alpha$ , the DE density parameter  $\Omega_{de,o}$  is determined. Here we rather use  $\Lambda$  and  $\Omega_{de,o}$  as independent parameters. In particular, numerical results are given for  $\Lambda = 10^3$  GeV.

The RP model with such  $\Lambda$  value is in slight disagreement with low- $l$  multipoles of the CMB anisotropy spectrum data. Agreement may be recovered with smaller  $\Lambda$ 's, which

however loose significance in particle physics. The SUGRA model considered here, on the contrary, is in fair agreement with all available data.

## REFERENCES

- Battye R. A. & Weller J., 2003, Phys.Rev., D68, 083506  
 Benson A. J., 2001, MNRAS, 325, 1039  
 Benson A. J., Baugh C. M., Cole S., Frenk C. S., Lacey C. G., 2000a, MNRAS, 316, 107  
 Benson A. J., Cole S., Frenk C. S., Baugh C. M., Lacey C. G., 2000b, MNRAS, 311, 793  
 Benson A. J., Frenk C. S., Baugh C. M., Cole S., Lacey C. G., 2003, MNRAS, 343, 679  
 Berlind A. A., Weinberg D. H., 2002, ApJ, 575, 587  
 Berlind A. A. et al., 2003, ApJ, 593, 1  
 Brax P. & Martin J., 1999, Phys.Lett., B468, 40  
 Brax P. & Martin J., 2000, Phys.Rev. D, 61, 103502  
 Brax P., Martin J. & Riazuelo A., 2000, Phys.Rev. D, 62, 103505  
 Bryan G.L. & Norman M.L., 1998, ApJ 495, 80  
 Bullock J. S., Wechsler R. H., Somerville R. S., 2002, MNRAS, 329, 246  
 De Bernardis P. et al., 2000, Nature 404, 955  
 Dolag K., Bartelmann M., Perrotta F., Baccigalupi C., Moscardini L., Meneghetti M., Tormen G., 2004, A&A, 416, 853  
 Dvali G., & Turner M., 2003, astro-ph/0301510  
 Efstathiou G. et al., 2002, MNRAS, 330, 29  
 Governato F., Baugh C. M., Frenk C. S., Cole S., Lacey C. G., Quinn T., Stadel J., 1998, Nature, 392, 359  
 Haiman Z., Mohr J. J. & Holder G. P., 2000, ApJ, 553, 545  
 Halverson N. W. et al., 2001 ApJ, 568, 38  
 Hanany S. et al., 2000, ApJ, 545, L5  
 Huterer D. & White M., 2002 ApJ, 578, L95  
 Jenkins A. et al., 2001, MNRAS, 321, 372  
 Kauffmann G., Nusser A., Steinmetz M., 1997, MNRAS, 286, 795  
 Kauffmann G., Colberg J. M., Diaferio A., White S. D. M., 1999a, MNRAS, 303, 188  
 Kauffmann G., Colberg J. M., Diaferio A., White S. D. M., 1999b, MNRAS, 307, 529  
 Klypin A., Macciò A.V., Mainini R., Bonometto S.A. 2003 ApJ, 599, 31  
 Knebe A., Kravtsov A. V., Gottloeber S., Klypin A., 2000, MNRAS, 317, 630  
 Kravtsov A., Klypin A. & Khokhlov A., 1997 ApJ, 111, 73 K  
 Kravtsov A. V., Berlind A. A., Wechsler R. H., Klypin A. A., Gottlöber A., Allgood B., Primack J. R., 2004, ApJ, 609, 35  
 Kuhlen, M., Strigari, L. E., Zentner, A. R., Bullock, J. S., & Primack, J. R. 2005, MNRAS, 357, 387  
 Linder E.V. & Jenkins A. 2003, MNRAS, 346, 573  
 Maccio' A. V., 2004, astro-ph/0402657 (MNRAS submitted)  
 Maccio' A. V., Governato F. & Horellou C., 2005, astro-ph/0412583 (MNRAS in press)  
 Magliocchetti M., Porciani C., 2003, MNRAS, 346, 186  
 Mainini R., Macciò A. V., Bonometto S. A., 2003a, NewAst., 8, 173  
 Mainini R., Macciò A. V., Bonometto S. A., Klypin A., 2003b ApJ, 599, 24  
 Majumdar S. & Mohr J. J., 2004, ApJ, 613, 41  
 Meneghetti M., Bartelmann M., Dolag K., Moscardini L., Perrotta F., Baccigalupi C., Tormen G., 2004, astro-ph/0405070 (A&A submitted)  
 Nagamine K., Fukugita M., Cen R., Ostriker J. P., 2001, ApJ, 558, 497  
 Pearce F. R., Jenkins A., Frenk C. S., White S. D. M., Thomas P. A., Couchman H. M. P., Peacock J. A., Efstathiou G., 2001, MNRAS, 326, 649  
 Percival W. J. et al., 2002, MNRAS, 337, 1068

- Perlmutter S. et al., 1999, ApJ, 517, 565  
Press W. H. & Schechter P., 1974, ApJ, 187, 425  
Ratra B., Peebles P. J. E., 1988, Phys.Rev.D, 37, 3406  
Riess, A. G. et al., 1998, AJ, 116, 1009  
Seljak U., 2000, MNRAS, 318, 203  
Sheth R. K. & Tormen G., 1999, MNRAS, 308, 119  
Sheth R. K. & Tormen G., 2002, MNRAS, 329, 61  
Sheth R. K., Diaferio A., 2001, MNRAS, 322, 901  
Somerville R. S., Lemson G., Sigad Y., Dekel A., Kauffmann G.,  
White S. D. M., 2001, MNRAS, 320, 289  
Spergel D. N. et al., 2003, ApJsuppl., 148, 175  
Tegmark, M., Zaldarriaga, M., Hamilton, A. J., 2001, Phys.  
Rev.D, 63, 43007  
Vale A. & Ostriker J.P., 2004, MNRAS, 353, 189V  
van den Bosch F.C, Yang X.H. & Mo H.J., 2003, MNRAS, 340,  
771  
Wang L. & Steinhardt P.J., 1998, ApJ, 508, 483  
Wechsler R. H., Somerville R. S., Bullock J. S., Kolatt T. S.,  
Primack J. R., Blumenthal G. R., Dekel A., 2001, ApJ, 554,  
85  
Wetterich C., 1988, Nucl.Phys.B, 302, 668  
Wetterich C., 1995 A&A 301, 32  
White M., Hernquist L., Springel V., 2001, ApJ, 550, L129  
Yang X.H., Mo H.J. & van den Bosch F.C, 2003, MNRAS, 339,  
1057  
Yang X.H., Mo H.J., Jing Y.P., van den Bosch F.C & Chu Y.,  
2004, MNRAS, 350, 1153  
Yoshikawa K., Taruya A., Jing Y. P., Suto Y., 2001, ApJ, 558,  
520  
Zheng Z., Tinker J. L., Weinberg D. H., Berlind A. A., 2002, ApJ,  
575, 617